

Short-range effects and magnetization reversal in $\text{Co}_{80}\text{Fe}_{20}$ thin films: a MOKE magnetometry/domain imaging and AMR study

J. M. Teixeira* and R.F.A. Silva, J. Ventura, A. Pereira, J. P. Araujo, M. Amado, F. Carpinteiro, J. B. Sousa

IFIMUP and DFFCUP, Rua do Campo Alegre, 678, 4169-007, Porto, Portugal

S. Cardoso, R. Ferreira and P. Freitas

INESC-MN and IST, Rua Alves Redol, 9-1, 1000-029 Lisbon, Portugal

A MOKE magnetometry unit simultaneously sensitive to both in-plane magnetization components, based on an intensity differential detection method, allows us to observe the uniaxial anisotropy impressed during CoFe-deposition and to discriminate the magnetization processes under a magnetic field parallel and perpendicular to such axes. Our MOKE imaging unit, using a CCD camera for Kerr effect domain visualization provides direct evidence on the dominant M-processes, namely domain wall motion and moment rotation. Further magnetic information was obtained by AMR measurements due to the dependence of the electrical resistivity on the short-range spin disorder and also on the angle between the electrical current direction (\mathbf{I}) and the spontaneous magnetization (\mathbf{M}_S).

Keywords: Tunnel Junction, Spin Valve, MOKE, Domain Imaging, AMR, Magnetic reversal

INTRODUCTION

Ferromagnetic CoFe films with appropriated composition provide highly spin-polarized 3d-electrons [1] enhancing the spin-dependent giant magnetoresistance. They are used in spintronic devices such as magnetic tunnel junctions [2], spin valves [3], sensitive magnetic sensors, high density read-heads [4] and non-volatile magnetic random access memories (MRAM) [5]. Magnetic switching and magnetization hysteresis is of particular relevance for device functionality.

Here we present a detailed study based on the Anisotropic Magnetoresistance (AMR), vectorial Magneto-Optical magnetometry and domain imaging of a series of 200 Å $\text{Co}_{80}\text{Fe}_{20}$ films with in-plane uniaxial anisotropy. A detailed description of these techniques is given.

The easy and hard axis magnetization curves, $M(H)$, are correlated with different orientational processes, as inferred from MOKE imaging. Further information was obtained from AMR measurements, due to their dependence on short-range spin disorder and on the angle between the electrical current direction and the spontaneous magnetization (\mathbf{M}_S). Under transverse magnetic fields, magnetic moment rotation dominate and lead to good correlation between M , AMR and domain patterns. For longitudinal fields the AMR(H) dependence cannot be correlated with $M(H)$ since significant AMR changes still occur when M is already saturated. Such changes are discussed in terms of short-range spin disorder effects.

EXPERIMENTAL DETAILS

The four probe technique was used for the AMR measurements, with the electric current along the long axis and the applied magnetic field parallel or at right angles to it. In ferromagnetic 3d-transition metals the electric resistivity depends on the angle θ between the electrical current and the spontaneous magnetization \mathbf{M}_S , through the so called anisotropic magnetoresistive effect (Smit mechanism; see [7]):

$$\rho(\mathbf{H}) = \rho_{\perp} + (\rho_{\parallel} - \rho_{\perp}) \cos^2 \theta, \quad (1)$$

*Electronic address: jmteixeira@fc.up.pt

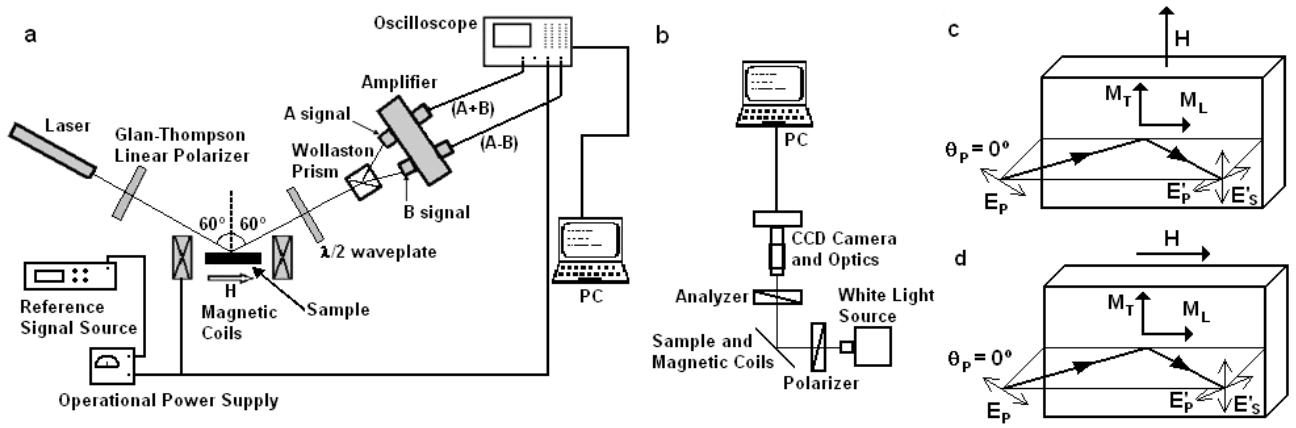


FIG. 1: (a) MOKE magnetometry system used in this work. (b) Domain imaging system. (c) Transverse MOKE geometry (d) Longitudinal MOKE geometry.

where ρ_\perp (ρ_\parallel) is the resistivity when \mathbf{M} is saturated perpendicular (parallel) to the electrical current. A magnetoresistive coefficient (at field \mathbf{H}) is defined as:

$$\frac{\Delta\rho}{\rho} = \frac{\rho(\mathbf{H}) - \rho(0)}{\rho(0)}. \quad (2)$$

For a film with \mathbf{M}_S in plane and starting with a random demagnetized state one has $\rho(0) = \frac{1}{2}\rho_\parallel + \frac{1}{2}\rho_\perp$. If the film has uniaxial anisotropy ($\pm\mathbf{M}_S$ domains) one simply has $\rho(0) = \rho_\parallel$. The so called anisotropic magnetoresistance ratio (AMR), is given by [7]:

$$AMR = \frac{\rho_\parallel - \rho_\perp}{\rho(0)}. \quad (3)$$

Using the vectorial MOKE magnetometer depicted in Fig. 1a we measured the technical magnetization $M(H)$ in the two common in-plane geometries [8]: the *transverse* geometry (Fig. 1c), with \mathbf{H} in the film plane and perpendicular to the laser beam incident plane; and the *longitudinal* geometry (Fig. 1d), in which the in-plane field is parallel to the incident plane. The light from a 5 mW He-Ne laser ($\lambda = 632.8$ nm) passes through a Glan-Thompson polarizer with an extinction ratio of 1×10^{-5} , giving linearly polarized light parallel (p -polarization) to the plane of incidence. The sample is located in the center of a pair of Helmholtz coils and in some situations between the poles of an electromagnet. When convenient, the (film) sample can be rotated in its plane. An operational current supply produces a periodic ($f=1$ Hz) magnetic field with triangular shape. The laser light falls at $\sim 60^\circ$ to the film normal, and after reflection passes through a $\lambda/2$ dielectric plate, resulting in a 45° rotation of the polarization plane. The light is then split into two beams by a Wollaston prism, corresponding to the two mutually orthogonal (s and p) components of the polarized light (A and B beams in Fig. 1a), and the corresponding intensities are measured by two independent photodiodes. Their outputs are connected to a locally built amplifier, providing the so called unbalanced and balanced MOKE signals. The unbalanced signal (difference between the s and p components, i.e. $A - B$ intensities) is proportional to the Kerr rotation and, in a first approximation, it is a linear function of the longitudinal (parallel to the plane of incidence) magnetization component (M_L ; Fig. 1). The balanced signal ($A + B$) is proportional to the square of the transversal (perpendicular to the plane of incidence) magnetization component (M_T ; Fig. 1). We can then simultaneously measure the parallel and perpendicular technical magnetization components, over the laser beam area, giving corresponding averages over the magnetic moments. A 4-channel digital oscilloscope is used to visualize and analyze the MOKE and the magnetic field signals. Each magnetization curve is obtained by averaging 128 successive hysteretic cycles.

A magnetic domain Kerr imaging system was also implemented to visualize the magnetic domains (Fig. 1b). High resolution image digital processing enables us to obtain the corresponding (averaged) technical magnetization. An halogen lamp provides a non coherent light beam for this imaging system. This light passes through a linear polarizer with the transmission axis parallel to the plane of incidence (p -polarization) and is reflected at an angle of $\sim 45^\circ$ with respect to the normal of the sample. A periodic triangular shape magnetic field is applied parallel to the film under study. An analyzer intercepts the reflected beam with its transmission axis perpendicular to the beam direction

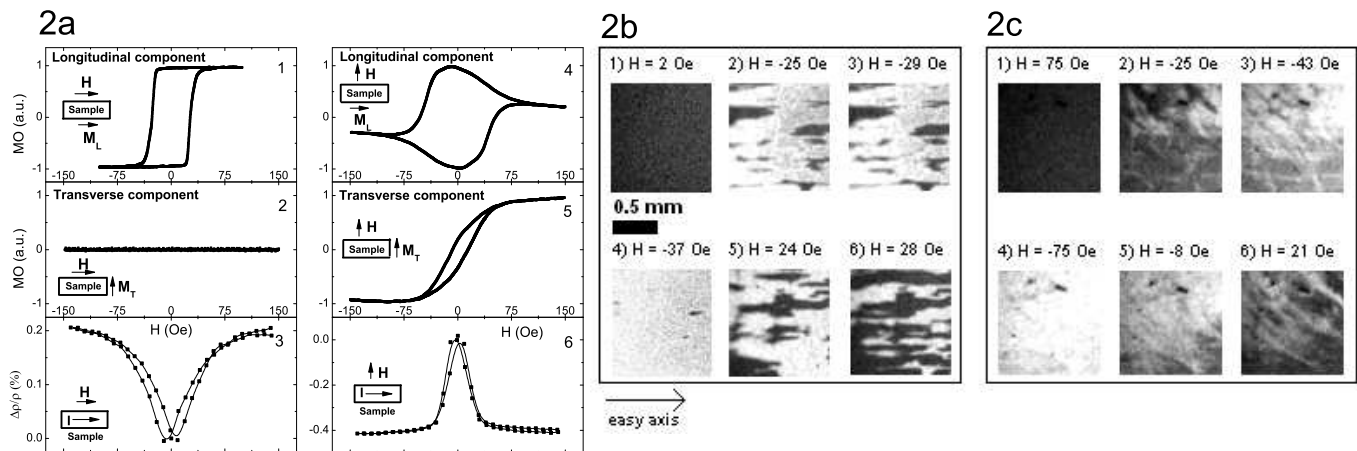


FIG. 2: MOKE and AMR curves for the $\text{Co}_{80}\text{Fe}_{20}$ annealed film with \mathbf{H} perpendicular [(a.4), (a.6) and (a.6)] and parallel [(a.1), (a.2) and (a.3)] to the scattering plane. (b) Magnetic domains in CoFe film along the forward (b.1)-(b.3) and backward (b.4)-(b.6) branches of the M_L loop depicted in a.1. ($\mathbf{H}_a //$ easy axis) (c) Magnetic domains along the forward (c.1)-(c.3) and backward (c.4)-(c.6) branches of the M_T loop depicted in a.5. (along hard axis)

and is adjusted to transmit only one component of the reflected light (the p - or s -component) [9]. A greyscale CCD camera with $\sim 10\mu\text{m}$ of resolution is used to acquire the magnetic domain images. Each image is saved in a bitmap format with 8 bit of information and is then subtracted from the magnetically saturated image to display only the features associated with the magnetic behavior. The magnetic field is produced by Helmholtz coils and acquired in an oscilloscope. The AMR and Kerr imaging units can operate simultaneously and are controlled (data acquisition and treatment) with a Labview program.

EXPERIMENTAL RESULTS

$\text{Co}_{80}\text{Fe}_{20}$ 200 Å thin rectangular (5×10 mm) films were grown on glass substrates by ion-beam deposition [6], and subsequently annealed for 10 min at 280°C . A magnetic field applied along the longitudinal direction during deposition (3 kOe) always impressed a magnetic easy axis.

MOKE magnetometry and imaging

Typical longitudinal and transverse Kerr hysteresis loops for the annealed CoFe film are presented in the four upper curves of Fig. 2, for an incident angle $\theta_i = 60^\circ$, using a p -polarized incident laser beam and covering the two in-plane MOKE geometries (see Figs. 1c, d).

For \mathbf{H} along the easy axis, the longitudinal component of the technical magnetization (M_L , Fig. 2a.1) exhibits a typical rectangular hysteretic cycle, whereas the transverse component M_T is zero (Fig. 2a.2; as expected for a soft ferromagnet magnetized along its easy axis). The $M_L(H)$ cycle indicates a magnetization process governed by sudden 180° -domain-wall propagation [10] (see below), leading to a coercive field $H_c \sim 27$ Oe and a saturation field $H_s \sim 50$ Oe.

For \mathbf{H} perpendicular to the easy axis, Fig. 2a.5 shows a narrow magnetization $M_T(H)$ cycle, which is typical along the hard axis. A small coercive field is observed ($H_c \sim 11$ Oe), whereas the saturation field is in this case much higher, $H_s \sim 75$ Oe. On the other hand, the behaviour of the longitudinal magnetization component (M_L , Fig. 2a.4) appears complex, with magnetization reversal at $H_c \sim 50$ Oe and $H_s \sim 90$ Oe.

AMR measurements

The magnetoresistance $\Delta\rho/\rho$ vs H curves for a magnetic field parallel or perpendicular to the electrical current [7] are shown in Figs. 2a.3 and 2a.6. The magnetoresistance is positive ($\Delta\rho/\rho \sim 0.2\%$) when the current and magnetic

field are parallel and negative ($\Delta\rho/\rho \sim -0.4\%$) when they are perpendicular; an AMR ratio of $\sim 0.6\%$ results from these data.

For the parallel configuration the $\Delta\rho/\rho$ curve saturates much later ($H_s \sim 150$ Oe) than in the perpendicular configuration ($H_s \sim 75$ Oe). In this context one also notices that under longitudinal fields the AMR(H) dependence does not correlate well with M(H) since important AMR changes still occur when M is saturated. Under transverse magnetic fields there is good agreement between M and AMR behaviour (see below).

ANALYSIS OF $M_T(H)$ AND $M_L(H)$ BEHAVIOR

The rectangular easy-axis magnetization curve in Fig. 2a.1 clearly indicates that the magnetization reversal is mainly due to sudden 180° -domain-wall formation and propagation, with no transverse magnetization component (M_T ; Fig.2a.2). This is directly confirmed by the domain images obtained in the forward (Fig. 2b.1→2b.3) and backward branches (Figs. 2b.4→2b.6) of the $M_L(H)$ loop. These sequences clearly demonstrate the nucleation of strip like magnetic domains, elongated along the easy axis, coexistent with magnetic domains of opposite magnetization (dark and bright regions), through 180° domain walls.

When the magnetic field is applied along the hard axis the growth of the transverse magnetization is quite gradual, as revealed by the intensity of the MOKE images (Figs. 2c.1→2c.6). This indicates the progressive rotation of the magnetization, as also reflected in the $M_L(H)$ dependence (Fig. 2a.4); for a strictly coherent rotation one would have $\tan\theta = M_T/M_L$.

AMR VERSUS M(H) BEHAVIOR

The magnetoresistance measurements show that this property is very sensitive to the type of magnetic processes underlying the magnetization reversal. Under transverse magnetic fields, when magnetization rotation processes dominate, we have a good correlation between the coercive and saturation fields extracted from the $M(H)$ and $AMR(H)$ curves. This indicates that the rotation processes, besides the magnetization, also dominate the variation of resistivity under transverse magnetic fields, through the Smit mechanism (eq.1). For this transverse field one still observes a longitudinal magnetization component, but it should vanish for a sufficiently high field. However, due to unavoidable small field misalignments with the hard axis, ultimate M_L vanishing is not strictly attained (Fig.2a.4). It can be shown that the $M_L(H)$ component undergoes in the hysteresis cycle a 360° in-plane rotation. At low fields the longitudinal magnetization component displays a maximum amplitude and the magnetoresistance is very small, since the magnetic moments are essentially along the easy axis ($\theta \approx 0$ or π ; $M_T/M_L \ll 1$) and, according to eq.1, $\rho(H) \sim \rho_{||} \sim \rho_0$ which leads to $\Delta\rho/\rho \sim 0$.

For longitudinal fields the AMR(H) dependence cannot be correlated with $M_L(H)$ since most of the AMR changes (Fig.2a.3) occur when M_L is already saturated (long-range magnetic order; Fig. 2a.1). Such pronounced AMR changes are therefore due to short-range spin disorder produced during the longitudinal magnetic switching, which persists well above H_s (as extracted from M_L). Within De Gennes-Friedel model [12] the spin disorder effects can be described by the expression $\rho(T, H) \simeq \rho_\infty [1 - \frac{M_S^2(T, H)}{M_S^2(0)} \frac{S}{S+1} + \sum f(R_{ij}) \langle \delta \vec{S}_i \cdot \delta \vec{S}_j \rangle_{T, H}]$, where ρ_∞ is the magnetic resistivity in the paramagnetic phase, $f(R_{ij})$ is the interference function for the scattered electron wavefunctions and $\langle \delta \vec{S}_i \cdot \delta \vec{S}_j \rangle$ is the correlation function for the spin fluctuations in different lattice sites \underline{i} and \underline{j} . For fully uncorrelated spin fluctuations (PM state or mean field FM state) one has $\langle \delta \vec{S}_i \cdot \delta \vec{S}_j \rangle = 0$. If one includes some degree of spin-spin correlation in the corresponding fluctuations, short range effects immediately affect $\rho(T, H)$, through $\langle \delta \vec{S}_i \cdot \delta \vec{S}_j \rangle \neq 0$. In this case, due to the small conduction electron wavelength (λ_F), only short-range effects are important in resistivity, i.e. in distances up to λ_F . This means the existence of short-range disorder effects in the nanometric range, considerably above H_s .

Work supported in part by POCTI/0155, IST-2001-37334 NEXT MRAM and POCTI/CTM/ 59318/2004 project. J. Ventura, R. Ferreira and S. Cardoso are thankful for FCT grants (SFRH/BD/7028/2001, SFRH/BD/6501/2001 and SFRH/BPD/7177/2001).

[1] Wohlfarth, *Ferromagnetic Materials; vol. 2*, North-Holland Company New York (1980).

- [2] J. S. Moodera, L. R. Kinder, T. M. Wong and R. Meservey, *Phys. Rev. Lett.* **74**, 3273 (1995).
- [3] J. B. Sousa *et al.*, *J. Appl. Phys.* **91**, 5321 (2002).
- [4] D. Song, J. Nowak, R. Larson, P. Kolbo, R. Chellew, *IEEE Trans. Magn.* **36** 2545 (2000).
- [5] S. Tehrani *et al.*, *IEEE Trans. Magn.* **36** 2752 (2000).
- [6] V. Gehanno *et al.*, *IEEE Trans. Magn.* **35**, 4361 (1999).
- [7] T. R. McGuire and R. I. Potter, *IEEE Trans. Magn.* **11**, 1018 (1975).
- [8] C. Daboo *et al.*, *Phys. Rev. B.* **47**, 11852 (1993).
- [9] J. M. Florczak and E. Dan Dahlberg, *J. Appl. Phys.* **67**, 7520 (1990).
- [10] Richard M. Bozorth, *Ferromagnetism*, IEEE Press (1951).
- [11] Alex Hubert and Rudolf Schäfer, *Magnetic Domains*, Springer (1998).
- [12] P.G. De Gennes and J. Friedel, *J. of Phys. Chem. Solids.* **4**, 71 (1958).